

Available online at www.sciencedirect.com**ScienceDirect**www.elsevier.com/locate/jes

JES
JOURNAL OF
ENVIRONMENTAL
SCIENCES
www.jesc.ac.cn

Hydrothermal-treated Pt/Al₂O₃ as an excellent catalyst for toluene total oxidation

Xiao Chen, Yong Wang, Jianyu Li, Zhongheng Hu, Ying Zhou, Huayan Liu,
Hanfeng Lu*

Institute of Catalytic Reaction Engineering, College of Chemical Engineering, Zhejiang University of Technology,
Hangzhou 310014, China

ARTICLE INFO

Article history:

Received 27 February 2021

Revised 26 June 2021

Accepted 28 June 2021

Available online 11 January 2022

Keywords:

Pt/Al₂O₃

Calcination activation

Hydrothermal activation

AlO(OH)

Catalytic combustion of toluene

ABSTRACT

The preparation of highly active supported noble metal catalysts with a low noble metal loading has always been the ultimate goal of researchers working on catalysis. Hydrothermally treated Pt/Al₂O₃ (Pt/Al₂O₃-H) exhibits better catalytic activity than that (Pt/Al₂O₃-C) treated via the conventional calcination approach. At the high space velocity of 100,000 mL/(g·hr), the temperature that correspond to 50% toluene conversion (T_{50}) of Pt/Al₂O₃-H is 115°C lower than that of Pt/Al₂O₃-C, and the turnover frequency (TOF) value can reach 0.0756 sec⁻¹. The mechanism by which the hydrothermal approach enhances Pt/Al₂O₃ activity has been investigated. The structure associated with the high catalytic activity of Pt nanoparticles (NPs) can be retained via hydrothermal treatment. Furthermore, the support is transformed to AlO(OH) with numerous surface hydroxyl groups, which in turn can facilitate the adsorption of toluene. And the synergistic effects of Pt NPs and AlO(OH) increases the contents of Pt in oxidation state and active oxygen, which are beneficial for toluene oxidation.

© 2022 The Research Center for Eco-Environmental Sciences, Chinese Academy of Sciences. Published by Elsevier B.V.

Introduction

Catalytic combustion of volatile organic compounds (VOCs) is an efficient and energy-saving process for VOCs elimination (Lu et al., 2015; Scirè and Liotta, 2012; Xie et al., 2016). Catalysts are at the heart of the catalytic combustion technology, which include supported noble metal catalysts (e.g., Pt, Pd, and Ru) and non-noble metal catalysts based on transition metals and rare earth metals (e.g., Mn, Cu, Co, Fe, and Ce) (Chen et al., 2018, 2017b; Garcia et al., 2006; Genuino et al., 2012; Gu et al., 2017; Pitkäaho et al., 2012; Tang et al., 2014). Although noble metals are scarce and expensive, supported noble metal catalysts, especially Pt-based catalysts, remain

the primary catalytic materials in practical applications owing to their superior catalytic activity, selectivity, and universality (Wang et al., 2020c; Zhang et al., 2020, 2019). Various supported noble metal catalysts that are highly active for VOCs combustion have been developed. Many supported Pt catalysts can achieve complete toluene conversion at temperatures (T_{90}) below 200°C (Huang et al., 2020; Kondratowicz et al., 2020; Lin et al., 2020; Lu et al., 2019; Pei et al., 2019; Rui et al., 2017; Yang et al., 2020, 2016; Zhang et al., 2018; Zou et al., 2020a, 2020b). However, researchers are further developing existing Pt catalysts that can completely convert toluene at lower temperatures to save on energy and ensure safety in practical applications. However, only a few the supported noble metal catalysts that can achieve complete toluene conversion at temperatures below 150°C, especially at high space velocities (no less than 100,000 mL/(g·hr)), have been reported.

* Corresponding author.

E-mail: luhf@zjut.edu.cn (H. Lu).

In addition, most of these catalysts attain such high activities under high noble metal loading (no less than 1 wt.%) (Huang et al., 2020; Lu et al., 2019; Zou et al., 2020a). Therefore, an obvious bottleneck in supported noble metal catalysts research is how to achieve high activity under low noble metal loading (Chen et al., 2019b; Huang et al., 2015; Sasaki et al., 2020; Wang et al., 2020b).

The impregnation method is a simple and widely used method for preparing supported noble metal catalysts (He et al., 2020; Sun et al., 2020; Zhu et al., 2018). In general, the performance of catalysts prepared via this method largely depends on the nature and characteristics of the support. By constructing a suitable support, an efficient supported noble metal catalyst can be prepared. Previous studies established that the size and dispersion of noble metals are crucial in determining the performance of supported noble metal catalysts (Chen et al., 2019a; Lai et al., 2014; Zhao et al., 2020b). Hence, only the nature of the support is considered in preparing supported noble metal catalysts, whereas the active structure of the noble metal is passively formed, thereby severely limiting the performance of catalysts. An ideal solution to enhancing catalytic activity is by preparing supported noble metal catalysts with controllable noble metals and supports. The colloid deposition method is a recently developed method for preparing inexpensive and highly active supported noble metal catalysts (Gan et al., 2019; Hashmi and Hutchings, 2006; Li et al., 2019). This method involves preforming noble metal nanoparticles (NPs) and depositing them on a specific support to form a supported noble metal catalyst. Via this method, the size and dispersion of preformed noble metal NPs can be effectively controlled, a feature that is beneficial to constructing highly active catalysts. Effective size and dispersion control can be achieved during colloid preparation by adding surfactants (Chen et al., 1999; Hirai et al., 1978). However, the presence of the surfactants is detrimental to catalytic activity. Consequently, the catalysts prepared via the colloid deposition method must be activated before they are used. The purpose of activation is to remove the surfactants to expose active sites. Current methods for catalyst activation typically involve thermal and oxidative treatments, which can affect the size or morphology of the noble metal NPs, in turn suppressing their catalytic activity (Chen et al., 2020; Goodman et al., 2019; Jia and Schüth, 2011; Wen et al., 2008; Yin et al., 2010; Zhou et al., 2009). Nevertheless, only the size and morphology of noble metal NPs are controlled, the performance of the catalyst can hardly be greatly improved by relying only on the activity of the noble metal NPs. Studies prove that the synergistic effects of noble metal NPs and supports are also crucial in determining catalyst performance (Boudart, 1969; Waqas et al., 2020; Zou et al., 2020b). So, in the activation process, while controlling the structure of the noble metal NPs, if the support of catalyst can also form a structure conducive to the reaction and assist in expressing the activity of noble metal NPs, it is very likely to considerably enhance the catalyst performance.

Al_2O_3 can be transformed into $\text{AlO}(\text{OH})$ with the special morphology and the abundant surface hydroxyl groups under hydrothermal condition (Kozerozhets et al., 2020; Li et al., 2010; Prorok and Madej, 2020). These features of $\text{AlO}(\text{OH})$ are beneficial to the catalytic combustion of VOCs (Belskaya et al., 2019; Cai et al., 2010; Chen et al., 2017a, 2017b; Xu et al., 2015).

Moreover, given that hydrothermal activation does not require further thermal treatment, the structure of noble metal NPs can be retained. In this study, $\text{Pt}/\text{Al}_2\text{O}_3$ were prepared via colloid deposition method. An innovation of this study was that the $\text{Pt}/\text{Al}_2\text{O}_3$ was activated via the hydrothermal approach to successfully prepare a highly efficient catalyst. The activity of the $\text{Pt}/\text{Al}_2\text{O}_3$ activated via the hydrothermal approach was substantially better than that of the catalyst prepared via traditional calcination activation. At the high space velocity of 100,000 mL/(g·hr), the T_{90} was only 150°C. The mechanism by which the hydrothermal approach activates the $\text{Pt}/\text{Al}_2\text{O}_3$ was determined and characterized via several approaches. This work reports a highly efficient Pt-based catalyst with low Pt loading. The results may provide insights into the design of highly efficient and inexpensive Pt-based catalysts.

1. Materials and methods

1.1. Chemical agents

Chloroplatinic acid hexahydrate ($\text{H}_2\text{PtCl}_6 \cdot 6\text{H}_2\text{O}$) was purchased Shanghai Aladdin Biochemical Technology Co., Ltd. Ascorbic acid ($\text{C}_6\text{H}_8\text{O}_6$) was purchased Shanghai Aladdin Biochemical Technology Co., Ltd. Polyvinylpyrrolidone ($(\text{C}_6\text{H}_9\text{NO})_n$, PVP) was purchased Shanghai Aladdin Biochemical Technology Co., Ltd. Ethylene glycol ($\text{C}_2\text{H}_6\text{O}_2$) was Shanghai Lingfeng Chemical Reagent Co., Ltd. Acetone ($\text{C}_3\text{H}_6\text{O}$) was purchased Hangzhou Shuanglin Chemical Reagent Co., Ltd. Ethanol ($\text{C}_2\text{H}_6\text{O}$) was purchased Anhui Ante Food Co., Ltd. Aluminum nitrate nonahydrate ($\text{Al}(\text{NO}_3)_3 \cdot 9\text{H}_2\text{O}$) was purchased Sinopharm Chemical Reagent Co., Ltd. Ammonia solution ($\text{NH}_3 \cdot \text{H}_2\text{O}$) was purchased Sinopharm Chemical Reagent Co., Ltd.

1.2. Catalyst preparation

Synthesis of Pt nanoparticle colloids: 0.03 g chloroplatinic acid hexahydrate, 1 g ascorbic acid and 0.9 g polyvinylpyrrolidone were mixed with 40 mL ethylene glycol in a three-necked flask. The mixture was heated to 180°C for 1 hr with magnetically stirred. After the reaction, acetone was added to the cooled solution to induce the precipitation of the nanoparticles, which were separated from the solvent by centrifugation at 8000 r/min for 10 min. The precipitation dispersed in ethanol, and then repeat the above operations several times. Finally, the resulting precipitation re-dispersed in 18 mL ethanol to form Pt nanoparticle colloids.

Pretreatment of Al_2O_3 support: 11.25 g $\text{Al}(\text{NO}_3)_3 \cdot 9\text{H}_2\text{O}$ was dissolved in 30 mL distilled water, and the PH was adjusted to 10 by using the $\text{NH}_3 \cdot \text{H}_2\text{O}$ solution (1 mol/L). After constant stirring for 2 hr at room temperature, the precipitation was separated from the solvent by pumping filtration. The precipitation was washed several times with distilled water, and then dried at 110°C for 12 hr. The resultant solid calcined at 500°C for 3 hr in the air atmosphere was denoted as Al_2O_3 .

Preparation of $\text{Pt}/\text{Al}_2\text{O}_3$ catalyst: 1 g Al_2O_3 and 8 mL Pt nanoparticle colloids were mixed with 10 mL ethanol. After constant stirring for 1 hr at room temperature, the mixture was allowed to stand overnight. The solid separated from the

mixture by pumping filtration, and then dried at 110°C for 2 hr was denoted as Pt/Al₂O₃ (theoretical Pt content: 0.5 wt.%). According to the different surfactant removal technology, the resultant catalysts were denoted as Pt/Al₂O₃-C and Pt/Al₂O₃-H, respectively.

Pt/Al₂O₃-C (calcination activation): Pt/Al₂O₃ was calcined at 400°C for 3 hr in the air atmosphere.

Pt/Al₂O₃-C (hydrothermal activation): Pt/Al₂O₃ was added to distilled water. After constant stirring at 90°C for 3 hr, the solid separated from the mixture by pumping filtration, and then dried at 110°C for 12 hr.

1.3. Catalyst characterization

Transmission electron microscope (Tecnai F30 S-Twin, Philips- FEI, Holland) working at 300 kV was used for transmission electron microscopy (TEM).

Scanning electron microscopy (SEM) images and energy dispersive spectrometer (EDS) were obtained on the scanning electron microscope (S-4700(II), Hitachi, Japan) operating at 15.0 kV.

X-ray diffraction (XRD) patterns were recorded on the diffractometer instrument (X'Pert PRO, Panalytical, Holland) operated at 40 kV and 30 mA, with Cu K α -ray radiation ($\lambda = 1.54178 \text{ \AA}$). Scans were taken with a 2 θ range from 10° to 80°.

N₂ adsorption-desorption isotherms of the samples were carried out at 77 K on the instrument (ASAP2020, Micromeritics, USA). The specific surface areas and the mesopore sizes of the samples were calculated using the Brunauer-Emmett-Teller (BET) and Barrett-Joyner-Halenda (BJH) method, respectively. All samples were pre-treated in vacuum at 200°C for 5 hr before measurements.

Raman spectra were acquired using a Raman spectrometer (HR 800 Lab RAM, Horiba Jobin Yvon, France) equipped with a 531.95 nm laser (frequency-doubled Nd:YAG, 20 mW).

X-ray photoelectron spectroscopy (XPS) was performed to identify the valence states and surface composition of the catalysts on the spectrometer (AXIS Ultra DLD, Kratos, England). The analysis system used a monochromatic Al Ka (1486.6 eV) X-ray source, and the pressure was kept below 5×10^{-7} Torr. The C 1 s peak (284.6 eV) was used to calibrate the binding energy (BE).

1.4. Catalytic performance test

Combustion of toluene activity over these catalysts was evaluated with a continuous flow-fixed bed reactor. The feed gas composed of 2500 ppmV toluene and balance standard air with a weight hourly space velocity (WHSV) of 100,000 mL/(g·hr), where the toluene was generated by bubbling standard air through a bottle contained pure toluene placed in an ice-water bath (0°C). The concentrations of the toluene were detected by a gas chromatograph (GC-2014, Shimadzu, Japan) equipped with flame ionization detector (FID). The conversion rate of toluene was obtained on the basis of toluene consumption, calculated by the inlet and outlet concentrations of toluene.

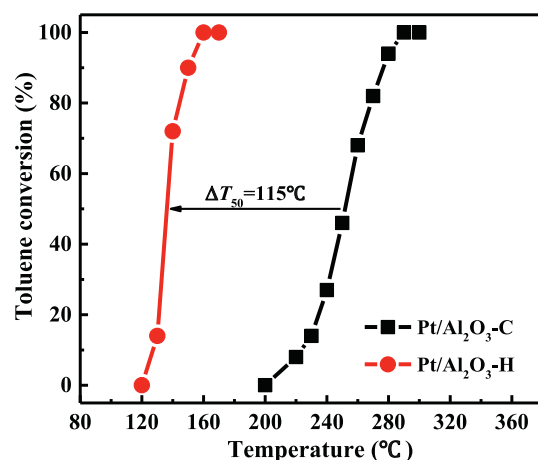


Fig. 1 – Toluene conversion as a function of temperature over the Pt/Al₂O₃-C (calcination activation) and Pt/Al₂O₃-H (hydrothermal activation). Reaction conditions: 2500 ppmV toluene, weight hour space velocity (WHSV) 100,000 mL/(g·hr). ΔT₅₀: the temperature that correspond to 50% toluene conversion.

Based on conversion rate of toluene, turnover frequency (TOF) was calculated by Eq. (1):

$$\text{TOF} = X_{\text{toluene}} \times F_{\text{toluene}} \times M_{\text{Pt}} / (m_{\text{cat}} \times X_{\text{Pt}} \times D_{\text{Pt}}) \quad (1)$$

where X_{toluene} is the conversion rate of toluene, F_{toluene} (mol/sec) is the flow rate of toluene, M_{Pt} (g/mol) is the molar mass of Pt, m_{cat} (g) is the mass of catalyst, X_{Pt} is the Pt content of catalyst, D_{Pt} is the Pt dispersion.

2. Results and discussion

2.1. Catalytic performance of Pt/Al₂O₃-C and Pt/Al₂O₃-H

The toluene catalytic combustion performance of Pt/Al₂O₃ activated by different approaches is depicted in Fig. 1. As shown in Figs. S1 and S2, the two approaches can effectively remove the PVP absorbed on Pt/Al₂O₃. Pt/Al₂O₃-H showed a better toluene catalytic combustion activity. Compared with Pt/Al₂O₃-C, the T₅₀ of Pt/Al₂O₃-H decreased by 115°C. The T₉₀ of Pt/Al₂O₃-H is only 150°C. Notably, the activity of Pt/Al₂O₃-H was better than that of most Pt-based catalysts (even with higher Pt contents) reported in the literature (Table 1). The value of TOF (Table S1), which was calculated with the dispersion of Pt loading on the support, over Pt/Al₂O₃-H and Pt/Al₂O₃-C was 0.0756 sec⁻¹ at 130°C and 0.0468 sec⁻¹ at 220°C, respectively, indicating that the active site on Pt/Al₂O₃-H had a higher catalytic ability. Compared with the catalyst activated via calcination, the Pt/Al₂O₃ activated via hydrothermal approach was more conductive to activity expression. In addition, as shown in Fig. S3, the toluene could also be completely oxidized to the CO₂ and H₂O over Pt/Al₂O₃-H.

Stability is another important indicator that measures catalyst performance. The stability of the Pt/Al₂O₃-H for toluene combustion was evaluated. As shown in Fig. 2a, the Pt/Al₂O₃-H exhibited similar catalytic activity within five reaction cy-

Table 1 – Complete toluene conversion at temperatures (T_{90}) of various Pt-based catalysts.

Sample	Toluene concentration (ppmV)	Space velocity (mL/(g·hr))	T_{90} (°C)	Reference
0.72 wt.%Pt/ZSM-5-OS	1000	120000	164	Huang et al., 2020
1.0 wt.%Pt/Ce _{0.2} CoO _x	1000	30000	173	Lin et al., 2020
1.0 wt.%Pt/ZF-D	1000	60000	148	Zou et al., 2020a
0.4 wt.%Pt/TiNT	500	30000	185	Rui et al., 2017
1.0 wt.%Pt/MOR	1000	60000	210	Zhang et al., 2018
0.5 wt.%Pt/Mn ₂ O ₃	1000	40000	240	Pei et al., 2019
0.93 wt.%Pt/KIT-6	500	80000	196	Yang et al., 2020
0.6 wt.%Pt/8.9 wt.%Co ₃ O ₄ /3DOM Al ₂ O ₃	1000	20000	200	Yang et al., 2016
1.4 wt.%Pt/DOM Al ₂ O ₃	1000	20000	197	Yang et al., 2016
2.1 wt.%Pt/TiO ₂ (PA)	1000	160000	165	Lu et al., 2019
2.0 wt.%Pt/TiO ₂ (CP)	1000	160000	187	Lu et al., 2019
0.66 wt.%Pt-I@Zr	1000	60000	279	Kondratowicz et al., 2020
0.57 wt.%Pt-G@Zr	1000	60000	172	Kondratowicz et al., 2020
0.48 wt.%Pt/Al ₂ O ₃ -H	2500	100000	150	This work

ZSM-5-OS: ellipsoidal ZSM-5 nanozeolit; ZF-D: pore-modified ZSM-5 foam; TiNT: TiO₂ nanotube arrays; MOR: mordenite; 3DOM Al₂O₃: three-dimensionally ordered macro-/mesoporous alumina; PA: platinum(II) acetylacetone; CP: chloroplatinic acid; Pt-I: impregnation used for modification with Pt; Pt-G: polyol process used for modification with Pt.

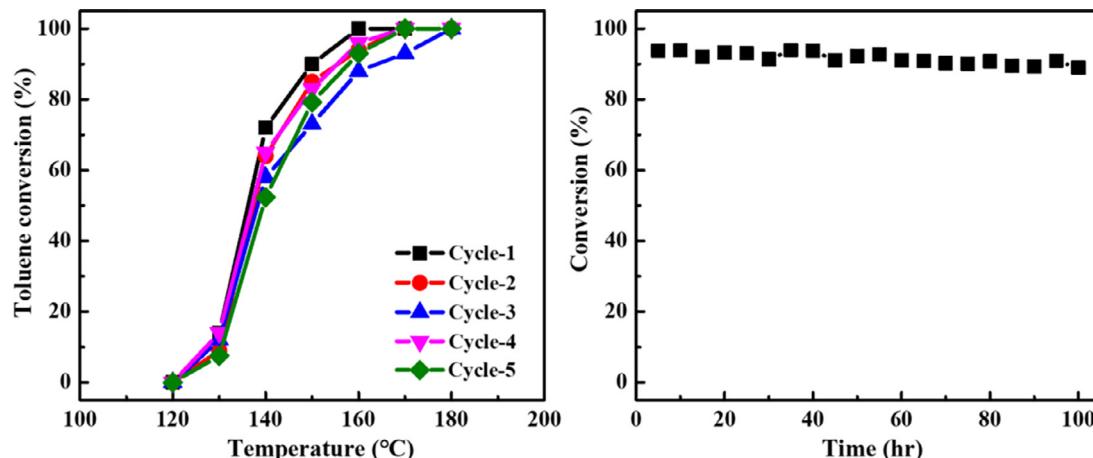


Fig. 2 – (a) Cycle test of Pt/Al₂O₃-H for toluene catalytic combustion; (b) Stability test of Pt/Al₂O₃-H for toluene catalytic combustion at 150°C. Reaction conditions: 2500 ppmV toluene, WHSV=100,000 mL/(g·hr).

cles, indicating the high stability of the Pt/Al₂O₃-H for toluene combustion. This property was also confirmed by a long-term reaction experiment. As shown in Fig. 2b, at the reaction temperature of 150°C, the Pt/Al₂O₃-H maintained a high and stable toluene conversion rate (about 90%). Only a small fluctuation was observed during the entire test period (100 hr). These results demonstrated the potential applications of the Pt/Al₂O₃-H.

2.2. Characterizations of Pt/Al₂O₃-C and Pt/Al₂O₃-H

Changes in the surface structures of Pt/Al₂O₃ activated by different approaches were monitored and characterized. TEM images and size histograms of the Pt/Al₂O₃-C and Pt/Al₂O₃-H are presented in Fig. 3. The Pt NPs of both samples were clearly well dispersed on the surface of the support. However, the size of Pt NPs in the Pt/Al₂O₃-C (4.22 nm) was larger than that in the Pt/Al₂O₃-H (2.69 nm). And the size and morphology of Pt NPs in the Pt/Al₂O₃-H did not substantially change

relative to those in the Pt colloids (2.45 nm, Fig. S4), indicating that hydrothermal activation did not have a considerable effect on the structure of the preformed noble metal NPs. Therefore, the active sites of the preformed noble metal NPs were retained. This achievement is useful in designing and synthesizing supported noble metal catalysts with a specific structure of noble metal to express high activity. Moreover, the morphology of the support in the Pt/Al₂O₃ activated by different approaches were vastly different. Accordingly, the Pt/Al₂O₃-C and Pt/Al₂O₃-H were characterized via SEM and XRD to investigate further the differences in the support of Pt/Al₂O₃ activated by different approaches.

SEM images of the Pt/Al₂O₃-C and Pt/Al₂O₃-H are given in Fig. 4a and b, respectively. Compared with the SEM images of Al₂O₃ (Fig. S4), calcination activation did not affect the morphology of the support, whereas hydrothermal activation resulted in the formation of numerous ridges on the surface of the sample. These ridges may provide a larger place for reaction. The effects of different activation approaches on the

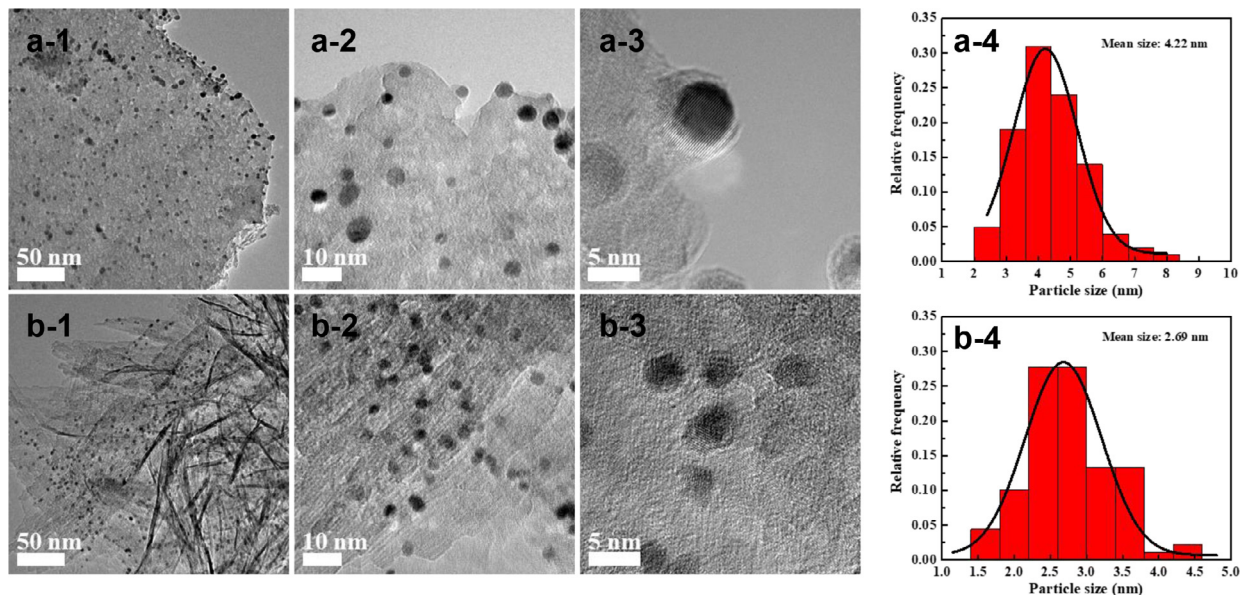


Fig. 3 – Transmission electron microscopy (TEM) images (1–3) and size histograms (4) of (a) Pt/Al₂O₃-C and (b) Pt/Al₂O₃-H.

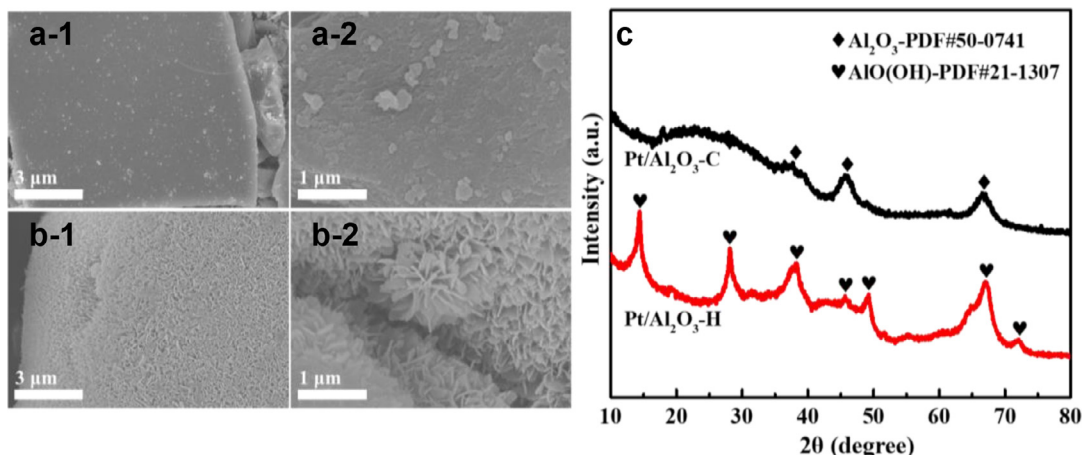


Fig. 4 – Scanning electron microscopy (SEM) images of (a) Pt/Al₂O₃-C and (b) Pt/Al₂O₃-H; (c) X-ray diffraction (XRD) patterns of Pt/Al₂O₃-C and Pt/Al₂O₃-H.

crystal phase of the support were determined. XRD patterns of the Pt/Al₂O₃-C and Pt/Al₂O₃-H are shown in Fig. 4c. Given that Pt content was low and highly dispersed, no characteristic peaks of Pt species were detected in the XRD of both samples. Therefore, the XRD patterns completely reflected the crystal phase of the support. Compared with the XRD patterns of Al₂O₃ (Fig. S5), calcination activation did not change the Al₂O₃ crystal phase of the support, whereas hydrothermal activation transformed the support from Al₂O₃ crystal phase to AlO(OH) crystal phase. AlO(OH) is an oxide with a layered structure (Fig. 4b). The special morphology and the existence of numerous surface hydroxyl groups of AlO(OH) facilitate toluene adsorption (Adebayo et al., 2020; Ncube et al., 2017; Qu et al., 2020). These features are some of the reasons the activity of the Pt/Al₂O₃-H was better than that of the Pt/Al₂O₃-C.

N₂ adsorption-desorption technique was adopted to evaluate the porous structure and texture of both samples.

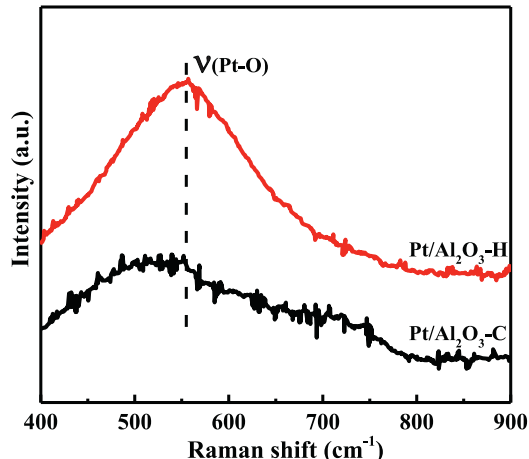
The adsorption-desorption isotherms and the corresponding pore-size distribution curves of the Pt/Al₂O₃-C and Pt/Al₂O₃-H are displayed in Fig. S6. It can be observed that both samples had similar mesoporous structures. However, the Pt/Al₂O₃-H had a larger specific surface area (S_{BET}), pore volume and pore size than the Pt/Al₂O₃-C (Table 2). These characteristics are more conducive to the adsorption and diffusion of reactants and products, thereby promoting the catalytic reaction. The diffusion of reactants in the Pt/Al₂O₃-C and Pt/Al₂O₃-H was further examined by establishing the corresponding surface diffusion model by using the Materials Studio software (Fig. S6). The surface diffusion factor (Table S2) of toluene on AlO(OH) (2.57) was greater than that on Al₂O₃ (1.20), indicating that the structure of Pt/Al₂O₃-H was more conducive to toluene diffusion than that of the Pt/Al₂O₃-C.

Above, the effects of different activation approaches on the activity of the catalysts were explored in terms of their phys-

Table 2 – Specific surface area (S_{BET}), pore volume, pore size, surface diffusion factor, and surface element composition of the Pt/Al₂O₃-C and Pt/Al₂O₃-H.

Sample	S_{BET} (m ² /g)	Pore volume (cm ³ /g)	Pore size (nm)	Surface element composition (Pt ⁴⁺ +Pt ^{δ+})/Pt _{total} (%)	O _{ads} /O _{total} (%)
Pt/Al ₂ O ₃ -C	135.5	0.98	4.38	29	61
Pt/Al ₂ O ₃ -H	208.8	3.47	6.24	46	75

O_{ads}: surface oxygen; O_{total}: the sum of lattice oxygen and surface oxygen.

**Fig. 5 – Raman spectra of Pt/Al₂O₃-C and Pt/Al₂O₃-H.**

ical structures. Pt was the active component of the catalysts. Therefore, the effects of different activation approaches on Pt NPs must be further evaluated. The Raman spectra of both samples are exhibited in Fig. 5. A broad peak is observed at 557 cm⁻¹, which was attributed to the stretching vibration of the Pt-O bond (Wang et al., 2019). The intensity of the vibration peak indicated that the Pt/Al₂O₃-H had more Pt-O bonds than Pt/Al₂O₃-C. This difference might be related to the interaction between Pt and the support. This supposition was further confirmed via XPS characterization.

The valence states of Pt NPs were characterized via XPS. Although the most intense photoemission lines of Pt were those that arose from Pt 4f levels, this energy region was overshadowed by the presence of a very strong Al 2p peak (Navarro et al., 2005). Consequently, the energy region of the less intense Pt 4d peak was recorded (Fig. 6a). After curve fitting, the Pt 4d peak of Pt/Al₂O₃-C was resolved into five peaks (Chen et al., 2017a; Jaramillo-Páez et al., 2018; Wang et al., 2013). The doublet peaks with binding energies of approximately 314.5 and 331.2 eV were assigned to the peaks of metallic Pt (Pt⁰); the doublet peaks with a binding energy of approximately 318.4 and 335.1 eV was assigned to the peaks of the oxidation state of Pt (Pt⁴⁺); and the single peak appeared at 325.2 eV which could be assigned to the peak of some partial oxidized state of Pt (Pt^{δ+}). For Pt/Al₂O₃-H, the Pt 4d peak was resolved into four peaks. The doublet peaks with binding energies of approximately 311.9 and 328.6 eV were assigned to the peaks of Pt⁰, and the doublet peaks with binding en-

ergies of approximately 315.8 and 332.5 eV were assigned to the peak of Pt⁴⁺. Compared with those in the Pt/Al₂O₃-C, the peak positions of Pt in Pt/Al₂O₃-H shifted to lower binding energies. This result was outcome probably because the support transformed from Al₂O₃ to AlO(OH), which in turn increased the negative electrons surrounding Pt. The contents of Pt at different valence states are listed in Table 2. The Pt/Al₂O₃-H had more abundant oxidized state of Pt (Pt⁴⁺+Pt^{δ+}) than the Pt/Al₂O₃-C possibly because the interaction between Pt and the support was stronger in the former than that in the latter. Given that the Pt colloids were synthesized under reducing conditions, metallic Pt was obtained. When the surfactant on the surface of Pt NPs was removed, the Pt NPs interacted with the support to change the valence state owing to their high surface energy. However, the interaction between the Pt NPs and the inert support Al₂O₃ was weak, and electron transfer did not readily occur between them. Therefore, the Pt/Al₂O₃ activated via calcination approach had only a small amount of Pt in oxidation state (Pt⁴⁺ and Pt^{δ+}). By contrast, AlO(OH) with incomplete crystallization and a high interfacial free energy exerted a strong interaction with the Pt NPs, which promoted the formation of Pt-O bands. Consequently, the Pt/Al₂O₃ activated via the hydrothermal approach had large amounts of Pt in oxidation state which were all Pt⁴⁺. Although the nature of active Pt species in the toluene combustion remains debatable, it has been recognized that either metallic Pt or synergistic metallic Pt and oxidized state of Pt are the active sites. A high Pt content in oxidation state helps to improve the catalytic activity of Pt-based catalysts (Cheng et al., 2020; Xi et al., 2020; Zhao et al., 2020a). This claim was consistent with the test results of toluene catalytic combustion over the Pt/Al₂O₃-C and Pt/Al₂O₃-H.

The O 1 s peaks of the Pt/Al₂O₃-C and Pt/Al₂O₃-H are shown in Fig. 6b. After curve fitting, the O 1 s peaks of both samples were resolved into two peaks. The peak with a binding energy of approximately 530.5 eV was assigned to the peak of lattice oxygen (O_{latt}), and the peak with a binding energy of approximately 531.6 eV was assigned to the peak of surface oxygen (O_{ads}). O_{ads} mainly include oxygen species, such as O₂²⁻, O⁻ and surface hydroxyl groups, which have good mobility and activity (Fan et al., 2017; Wang et al., 2020a; Wei et al., 2011). The Pt/Al₂O₃-H had more O_{ads} on its surface than the Pt/Al₂O₃-C (Table 2) because AlO(OH) had abundant surface hydroxyl groups and strongly interacted with the Pt NPs. Pt NPs in Pt/Al₂O₃-H were easier to activate adsorbed O₂ than those in Pt/Al₂O₃-C (Jeong et al., 2008; Zhang et al., 2012), thus benefitting the catalytic combustion of toluene.

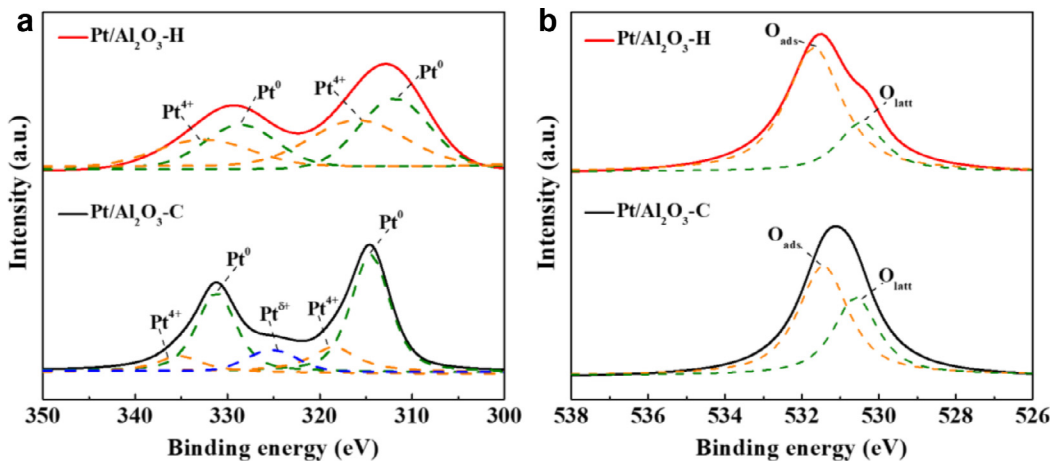


Fig. 6 – (a) Pt 4d and (b) O 1 s X-ray photoelectron spectroscopy (XPS) spectra of Pt/Al₂O₃-C and Pt/Al₂O₃-H.

2.3. Mechanism for improving performance of Pt/Al₂O₃ activated by hydrothermal approach

According to above results, the possible mechanism by which the hydrothermal approach activates the as-prepared Pt/Al₂O₃ catalyst with excellent performance of catalytic toluene combustion could be inferred. Catalytic toluene combustion is determined by three main factors (Gan et al., al., 2019): toluene adsorption, O₂ activation, and desorption products (CO₂ and H₂O). In this work, Al₂O₃ is transformed into AlO(OH) by hydrothermal activation, thereby endowing the catalysts with abundant surface hydroxyl groups and substantially improving their toluene adsorption capacity. AlO(OH) has a larger specific surface area than Al₂O₃ owing to its special morphology and structure that facilitates toluene adsorption. The strong interaction between AlO(OH) and Pt NPs promoted electron transfer between them, making the activation of adsorbed O₂ by Pt easier. The synergistic effects of Pt NPs and AlO(OH) promoted the toluene oxidation process. Moreover, according to the results of stability test in Fig. 2, the reaction products desorbed well on Pt/Al₂O₃-H. Therefore, the Pt/Al₂O₃-H exhibited excellent toluene catalytic combustion activity and stability. In sum, the structure of hydrothermally treated Pt/Al₂O₃ is suitable for toluene oxidation. The possible reaction process by which the Pt/Al₂O₃-H catalyzes toluene combustion is illustrated in Fig. 7. Hydrothermal treatment induces the as-prepared Pt/Al₂O₃ to produce abundant surface hydroxyl groups, and the Pt NPs in this structure more easily activate the adsorbed O₂ into active oxygen species. And, the abundant surface hydroxyl groups of the catalyst facilitate toluene adsorption. Afterward, the active oxygen species oxidize the adsorbed toluene to CO₂ and H₂O. Finally, CO₂ and H₂O are desorbed from the catalyst surface, allowing the catalyst to resume its activity.

2.4. Improving performance of Pt/Al₂O₃-C by hydrothermal treatment

We predicted that the support of Pt/Al₂O₃-C treated via the hydrothermal approach (denoted as Pt/Al₂O₃-C-H) would transform from Al₂O₃ to AlO(OH) and interact with the Pt NPs to en-

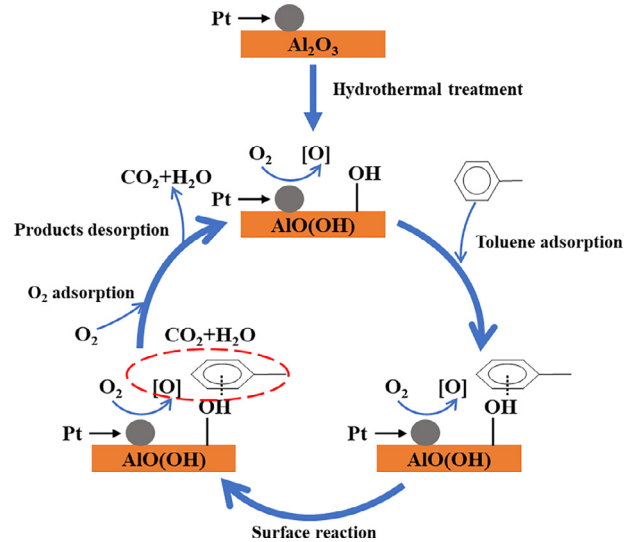


Fig. 7 – A proposed reaction process of toluene oxidation over Pt/Al₂O₃-H.

hance the catalytic performance of toluene combustion. The proposed mechanism was verified by comparing the predicted results with the actual characterization and activity test results of Pt/Al₂O₃-C-H.

The XRD pattern and SEM image of the Pt/Al₂O₃-C-H are shown in Fig. 8a. The crystalline phase structure and morphology of the Pt/Al₂O₃-C-H were consistent with those of Pt/Al₂O₃-H. Compared with Pt/Al₂O₃-C (Table 2), the Pt/Al₂O₃-C-H had a larger S_{BET} (176.7 m²/g), pore volume (2.76 cm³/g), and pore size (5.47 nm). These results demonstrated that the support of the Pt/Al₂O₃-C treated via hydrothermal approach transformed from Al₂O₃ to AlO(OH), consistent with the predicted results. The Raman spectrum (Fig. 8b) of the Pt/Al₂O₃-C-H shows that the intensity of the Pt–O bond stretching vibration peak was considerably stronger than that of the Pt/Al₂O₃-C, indicating that the interaction between the Pt NPs and the support was enhanced after the Pt/Al₂O₃-C treated via hydrothermal approach. This result was also confirmed by the XPS spectrum of the Pt/Al₂O₃-C-H (Fig. 8c and d). Compared

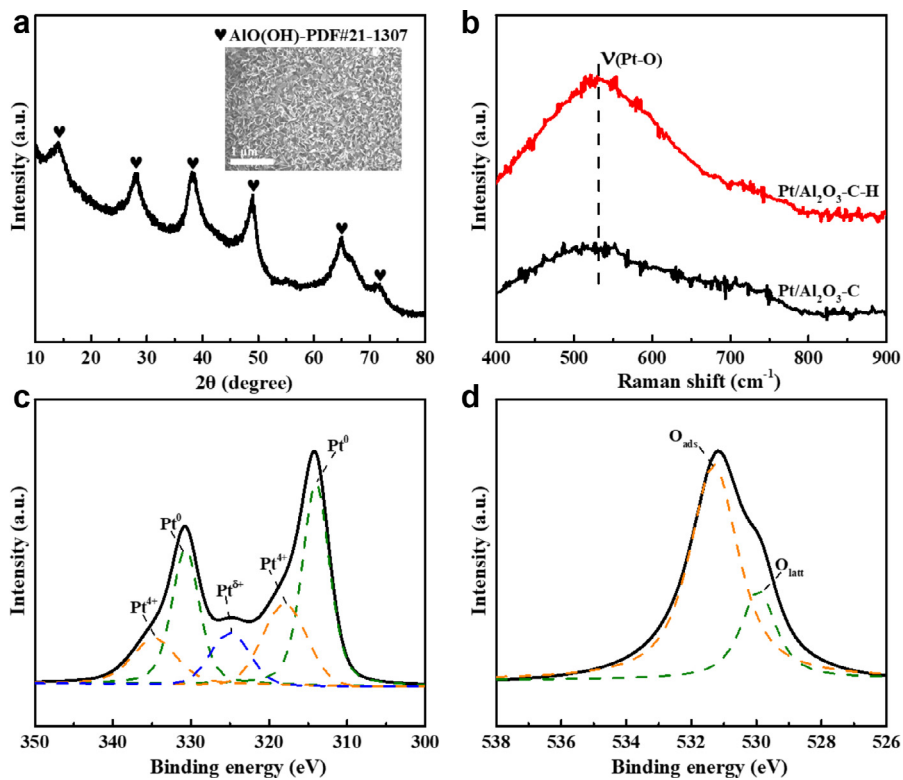


Fig. 8 – (a) XRD patterns, (inset) SEM images, **(b)** Raman, **(c)** Pt 4d and **(d)** O 1 s XPS spectra of Pt/Al₂O₃-C-H (Pt/Al₂O₃-C treated via the hydrothermal approach).

with those of the Pt/Al₂O₃-C (**Table 2**), the Pt in oxidation and O_{ads} contents of the Pt/Al₂O₃-C-H substantially increased to 42% and 77%, respectively. These results showed that the support of the Pt/Al₂O₃-C treated via hydrothermal approach strongly interacted with Pt NPs, consistent with the predicted results.

The catalytic toluene combustion performance of the Pt/Al₂O₃-C and Pt/Al₂O₃-C-H is presented in **Fig. 9**. As expected, Pt/Al₂O₃-C-H had a better catalytic toluene combustion activity than the Pt/Al₂O₃-C. Compared with that of the Pt/Al₂O₃-C, the toluene catalytic combustion (*T*₅₀) of the Pt/Al₂O₃-C-H decreased by 89°C. This result proved that hydrothermal treatment of Pt/Al₂O₃ is a feasible strategy for enhancing the catalytic activity in toluene combustion. However, the activity of the Pt/Al₂O₃-C-H (0.0540 sec⁻¹ at 140°C, **Table S1**) was lower than that of Pt/Al₂O₃-H (0.0756 sec⁻¹ at 130°C, **Table S1**). This result was obtained probably because the as-prepared Pt/Al₂O₃ activated via calcination approach reduced the surface energy of Pt NPs, thereby weakening the interaction between the Pt NPs and AlO(OH). Moreover, this result indicated that hydrothermal activation would not substantially affect the Pt NPs, and the structure associated with the high activity of the Pt NPs can be retained.

3. Conclusions

In summary, we obtained a highly efficient catalyst by activating Pt/Al₂O₃ via the hydrothermal approach. Its excellent ac-

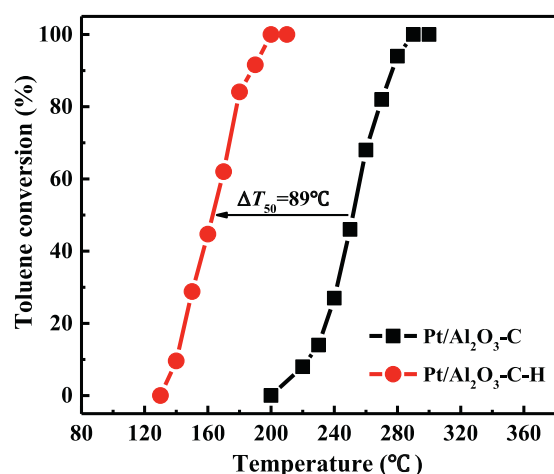


Fig. 9 – Toluene conversion as a function of temperature over the Pt/Al₂O₃-C and Pt/Al₂O₃-C-H. Reaction conditions: 2500 ppmV toluene, WHSV=100,000 mL/(g·hr).

tivity was due to the synergistic effects of Pt NPs and AlO(OH). Unlike calcination activation (which requires thermal treatment), hydrothermal activation did not considerably increase the size of Pt NPs, thereby retaining the structure associated with high catalytic activity of the Pt NPs. Moreover, the support of the Pt/Al₂O₃ activated via the hydrothermal approach was transformed from Al₂O₃ to AlO(OH) with a special morphology and abundant surface hydroxyl groups. The strong

interaction between the Pt NPs and AlO(OH) increased the Pt content in oxidation state and more easily activated the adsorbed O₂. The presence of abundant surface hydroxyl groups facilitated toluene adsorption to promote the toluene oxidation process. This study provides insights into the design of highly efficient and inexpensive Pt-based catalysts.

Acknowledgments

This work was supported by the National Natural Science Foundation of China (Nos. 21506194, 21676255) and the Zhejiang Provincial Natural Science Foundation of China (Nos. LZ21E080001, 2017C03007, 2017C33106).

Appendix A Supplementary data

Supplementary data associated with this article can be found in the online version at doi:[10.1016/j.jes.2021.06.031](https://doi.org/10.1016/j.jes.2021.06.031).

REFERENCES

- Adebayo, B.O., Krishnamurthy, A., Rownaghi, A.A., Rezaei, F., 2020. Toluene abatement by simultaneous adsorption and oxidation over mixed-metal oxides. *Ind. Eng. Chem. Res.* 59, 13762–13772.
- Belskaya, O.B., Leont'eva, N.N., Zaikovskii, V.I., Kazakov, M.O., Likholobov, V.A., 2019. Synthesis of layered magnesium-aluminum hydroxide on the γ -Al₂O₃ surface for modifying the properties of supported platinum catalysts. *Catal. Today* 334, 249–257.
- Boudart, M., 1969. Catalysis by supported metals. *Adv. Catal.* 20, 153–166.
- Cai, W.Q., Yu, J.G., Gu, S.H., Jaroniec, M., 2010. Facile hydrothermal synthesis of hierarchical boehmite: sulfate-mediated transformation from nanoflakes to hollow microspheres. *Cryst. Growth Des.* 10, 3977–3982.
- Chen, C.W., Tano, D., Akashi, M., 1999. Synthesis of platinum colloids sterically stabilized by poly(N-vinylformamide) or poly(N-vinylalkylamide) and their stability towards salt. *Colloid Polym. Sci.* 277, 488–493.
- Chen, F., Wang, F., Li, Q., Cao, C.Y., Zhang, X., Ma, H., et al., 2017a. Effect of support (Degussa P25 TiO₂, anatase TiO₂, γ -Al₂O₃, and AlOOH) of Pt-based catalysts on the formaldehyde oxidation at room temperature. *Catal. Commun.* 99, 39–42.
- Chen, L.N., Hou, K.P., Liu, Y.S., Qi, Z.Y., Zheng, Q., Lu, Y.H., et al., 2019a. Efficient hydrogen production from methanol using a single-site Pt₁/CeO₂ catalyst. *J. Am. Chem. Soc.* 141, 17995–17999.
- Chen, X., Li, J.Y., Wang, Y., Zhou, Y., Zhu, Q.L., Lu, H.F., 2020. Preparation of nickel-foam-supported Pd/NiO monolithic catalyst and construction of novel electric heating reactor for catalytic combustion of VOCs. *Appl. Catal. A* 607, 117839.
- Chen, X., Xu, Q.Q., Zhou, Y., Zhu, Q.L., Huang, H.F., Pan, Z.Y., et al., 2017b. Facile and flexible preparation of highly active CuCe monolithic catalysts for VOCs combustion. *ChemistrySelect* 2, 9069–9073.
- Chen, X., Zhao, Z.L., Zhou, Y., Zhu, Q.L., Pan, Z.Y., Lu, H.F., 2018. A facile route for spraying preparation of Pt/TiO₂ monolithic catalysts toward VOCs combustion. *Appl. Catal. A* 566, 190–199.
- Chen, Z.Y., Mao, J.X., Zhou, R.X., 2019b. Preparation of size-controlled Pt supported on Al₂O₃ nanocatalysts for deep catalytic oxidation of benzene at lower temperature. *Appl. Surf. Sci.* 465, 15–22.
- Cheng, Z., Feng, B.B., Chen, Z., Zheng, J., Li, J., Zuo, S.F., 2020. La₂O₃ modified silica-pillared clays supported PtO_x nanocrystalline catalysts for catalytic combustion of benzene. *Chem. Eng. J.* 392, 123747.
- Fan, L.J., Xi, K., Zhou, Y., Zhu, Q.L., Chen, Y.F., Lu, H.F., 2017. Design structure for CePr mixed oxide catalysts in soot combustion. *RSC Adv.* 7, 20309–20319.
- Gan, T., Chu, X.F., Qi, H., Zhang, W.X., Zou, Y.C., Yan, W.F., et al., 2019. Pt/Al₂O₃ with ultralow Pt-loading catalyze toluene oxidation: promotional synergistic effect of Pt nanoparticles and Al₂O₃ support. *Appl. Catal. B* 257, 117943.
- García, T., Solsona, B., Taylor, S.H., 2006. Naphthalene total oxidation over metal oxide catalysts. *Appl. Catal. B* 66, 92–99.
- Genuino, H.C., Dharmarathna, S., Nijagi, E.C., Mei, M.C., Suib, S.L., 2012. Gas-phase total oxidation of benzene, toluene, ethylbenzene, and xylenes using shape-selective manganese oxide and copper manganese oxide catalysts. *J. Phys. Chem. C* 116, 12066–12078.
- Goodman, E.D., Ye, A.A., Aitbekova, A., Mueller, O., Riscoe, A.R., Taylor, T.N., et al., 2019. Palladium oxidation leads to methane combustion activity: effects of particle size and alloying with platinum. *J. Chem. Phys.* 151, 154703.
- Gu, L., Chen, X., Zhou, Y., Zhu, Q.L., Huang, H.F., Lu, H.F., 2017. Propene and CO oxidation on Pt/Ce-Zr-SO₄²⁻ diesel oxidation catalysts: effect of sulfate on activity and stability. *Chin. J. Catal.* 38, 607–615.
- Hashmi, A.S.K., Hutchings, G.J., 2006. Gold catalysis. *Angew. Chem. Int. Ed.* 45, 7896–7936.
- He, L., Fan, Y.L., Luo, L.G., Bellettre, J., Yue, J., 2020. Preparation of Pt/ γ -Al₂O₃ catalyst coating in microreactors for catalytic methane combustion. *Chem. Eng. J.* 380, 122424.
- Hirai, H., Nakao, Y., Toshima, N., 1978. Preparation of colloidal rhodium in poly(vinyl alcohol) by reduction with methanol. *J. Macromol. Sci. Chem.* 12, 1117–1141.
- Huang, H.F., Jiang, B., Gu, L., Qi, Z.H., Lu, H.F., 2015. Promoting effect of vanadium on catalytic activity of Pt/Ce-Zr-O diesel oxidation catalysts. *J. Environ. Sci.* 33, 135–142.
- Huang, S.S., Yang, D.Y., Tang, Q.X., Deng, W., Zhang, L., Jia, Z.Y., et al., 2020. Pt-loaded ellipsoidal nanozeolite as an active catalyst for toluene catalytic combustion. *Microporous Mesoporous Mater.* 305, 110292.
- Jaramillo-Páez, C.A., Navío, J.A., Hidalgo, M.C., Macías, M., 2018. ZnO and Pt-ZnO photocatalysts: characterization and photocatalytic activity assessing by means of three substrates. *Catal. Today* 313, 12–19.
- Jeong, J.W., Choi, B., Lim, M.T., 2008. Catalytic oxidation for carbon-black simulating diesel particulate matter over promoted Pt/Al₂O₃ catalysts. *J. Ind. Eng. Chem.* 14, 830–835.
- Jia, C.J., Schüth, F., 2011. Colloidal metal nanoparticles as a component of designed catalyst. *Phys. Chem. Chem. Phys.* 13, 2457–2487.
- Kondratowicz, T., Drodzdek, M., Michalik, M., Gac, W., Gajewska, M., Kuśtrowski, P., 2020. Catalytic activity of Pt species variously dispersed on hollow ZrO₂ spheres in combustion of volatile organic compounds. *Appl. Surf. Sci.* 513, 145788.
- Kozerzhets, I.V., Panasyuk, G.P., Semenov, E.A., Voroshilov, I.L., Azarova, L.A., Belan, V.N., 2020. Mechanism of the conversion of γ -Al₂O₃ nanopowder into boehmite under hydrothermal conditions. *Inorg. Mater.* 56, 716–722.
- Lai, Y.T., Chen, T.C., Lan, Y.K., Chen, B.S., You, J.H., Yang, C.M., et al., 2014. Pt/SBA-15 as a highly efficient catalyst for catalytic toluene oxidation. *ACS Catal.* 4, 3824–3836.
- Li, H.T., Xu, Y.L., Gao, C.G., Zhao, Y.X., 2010. Structural and textural evolution of Ni/ γ -Al₂O₃ catalyst under hydrothermal conditions. *Catal. Today* 158, 475–480.

- Li, L.C., Zhang, N.Q., He, H., Zhang, G.Z., Song, L.Y., Qiu, W.G., 2019. Shape-controlled synthesis of Pd nanocrystals with exposed {110} facets and their catalytic applications. *Catal. Today* 327, 28–36.
- Lin, Y., Sun, J., Li, S.J., Wang, D., Zhang, C.H., Wang, Z., et al., 2020. An efficient Pt/Ce_yCoO_x composite metal oxide for catalytic oxidation of toluene. *Catal. Lett.* 150, 3206–3213.
- Lu, A.L., Sun, H.L., Zhang, N.W., Che, L.M., Shan, S.Y., Luo, J., et al., 2019. Surface partial-charge-tuned enhancement of catalytic activity of platinum nanocatalysts for toluene oxidation. *ACS Catal.* 9, 7431–7442.
- Lu, H.F., Kong, X.X., Huang, H.F., Zhou, Y., Chen, Y.F., 2015. Cu–Mn–Ce ternary mixed-oxide catalysts for catalytic combustion of toluene. *J. Environ. Sci.* 32, 102–107.
- Navarro, R.M., Álvarez-Galván, M.C., Sánchez-Sánchez, M.C., Rosa, F., Fierro, J.L.G., 2005. Production of hydrogen by oxidative reforming of ethanol over Pt catalysts supported on Al₂O₃ modified with Ce and La. *Appl. Catal. B* 55, 229–241.
- Ncube, T., Reddy, K.S.K., Shoaibi, A.S.A., Srinivasakannan, C., 2017. Benzene, Toluene, m-Xylene adsorption on silica-based adsorbents. *Energy Fuels* 31, 1882–1888.
- Pei, W.B., Liu, Y.X., Deng, J.G., Zhang, K.F., Hou, Z.Q., Zhao, X.T., et al., 2019. Partially embedding Pt nanoparticles in the skeleton of 3DOM Mn₂O₃: an effective strategy for enhancing catalytic stability in toluene combustion. *Appl. Catal. B* 256, 117814.
- Pitkäaho, S., Matejova, L., Ojala, S., Gaalova, J., Keiski, T.L., 2012. Oxidation of perchloroethylene—Activity and selectivity of Pt, Pd, Rh, and V₂O₅ catalysts supported on Al₂O₃, Al₂O₃–TiO₂ and Al₂O₃–CeO₂. *Appl. Catal. B* 113–114, 150–159.
- Prorok, R., Madej, D., 2020. Influence of hydrothermal conditions on the phase composition of materials from the system MgO–Al₂O₃–SiO₂–H₂O. *J. Aust. Ceram. Soc.* 56, 829–837.
- Qu, J.F., Chen, D.Y., Li, N.J., Xu, Q.F., Li, H., He, J.H., et al., 2020. Construction of Pd-modified NiCoOx hollow nanospheres with surface hydroxyls and oxygen vacancies for highly enhanced catalytic toluene oxidation activity. *ACS Sustain. Chem. Eng.* 8, 10581–10587.
- Rui, Z.B., Tang, M.N., Ji, W.K., Ding, J.J., Ji, H.B., 2017. Insight into the enhanced performance of TiO₂ nanotube supported Pt catalyst for toluene oxidation. *Catal. Today* 297, 159–166.
- Sasaki, T., Horino, Y., Otake, T., Ogawa, K., Suzuki, Y., 2020. A highly efficient monolayer Pt nanoparticle catalyst prepared on a glass fiber surface. *Catalysts* 10, 472.
- Scirè, S., Liotta, L.F., 2012. Supported gold catalysts for the total oxidation of volatile organic compounds. *Appl. Catal. B* 125, 222–246.
- Sun, M., Hu, W., Yuan, S.D., Zhang, H.L., Cheng, T.Q., Wang, J.L., et al., 2020. Effect of the loading sequence of CeO₂ and Pd over Al₂O₃ on the catalytic performance of Pd-only close-coupled catalysts. *Mol. Catal.* 482, 100332.
- Tang, W.X., Wu, X.F., Li, S.D., Li, W.H., Chen, Y.F., 2014. Porous Mn–Co mixed oxide nanorod as a novel catalyst with enhanced catalytic activity for removal of VOCs. *Catal. Commun.* 56, 134–138.
- Wang, F., Qi, G.Q., Zhang, C.Q., Ren, H.C., Ma, H., Guo, Y., 2020a. Na-promoted Pt/Al₂O₃ activity stability for the complete oxidation of HCHO at room temperature. *Catal. Commun.* 139, 105713.
- Wang, M.M., Chen, D.Y., Li, N.J., Xu, Q.F., Li, H., He, J.H., et al., 2020b. Highly efficient catalysts of bimetallic Pt–Ru nanocrystals supported on ordered ZrO₂ nanotube for toluene oxidation. *ACS Appl. Mater. Interfaces* 12, 13781–13789.
- Wang, X.D., Yu, H.B., Hua, D.Y., Zhou, S.H., 2013. Enhanced catalytic hydrogenation activity and selectivity of Pt–M_xO_y/Al₂O₃ (M=Ni, Fe, Co) heteroaggregate catalysts by in situ transformation of PtM alloy nanoparticles. *J. Phys. Chem. C* 117, 7294–7302.
- Wang, Y.H., Le, J.B., Li, W.Q., Wei, J., Radjenovic, P.M., Zhang, H., et al., 2019. In situ spectroscopic insight into the origin of the enhanced performance of bimetallic nanocatalysts towards the oxygen reduction reaction (ORR). *Angew. Chem. Int. Ed.* 58, 16062–16066.
- Wang, Z.W., Ma, P.J., Zheng, K., Wang, C., Liu, Y.X., Dai, H.X., et al., 2020c. Size effect, mutual inhibition and oxidation mechanism of the catalytic removal of a toluene and acetone mixture over TiO₂ nanosheet-supported Pt nanocatalysts. *Appl. Catal. B* 274, 118963.
- Waqas, M., Kasmi, A.E., Kouotou, P.M., Wang, Y., Tian, Z.Y., 2020. Support effect on the catalytic activity and stability of non-crystal ternary oxides. *Colloids Surf. A* 586, 124218.
- Wei, Y.C., Liu, J., Zhao, Z., Chen, Y.S., Xu, C.M., Duan, A.J., et al., 2011. Highly active catalysts of gold nanoparticles supported on three-dimensionally ordered macroporous LaFeO₃ for soot oxidation. *Angew. Chem., Int. Ed.* 50, 2326–2329.
- Wen, L., Fu, J.K., Gu, P.Y., Yao, B.X., Lin, Z.H., Zhou, J.Z., 2008. Monodispersed gold nanoparticles supported on γ-Al₂O₃ for enhancement of low-temperature catalytic oxidation of CO. *Appl. Catal. B* 79, 402–409.
- Xi, K., Wang, Y., Jiang, K., Xie, J., Zhou, Y., Lu, H.F., 2020. Support interaction of Pt/GeO₂ and Pt/SiC catalysts prepared by nano platinum colloid deposition for CO oxidation. *J. Rare Earths* 38, 376–383.
- Xie, Y.J., Guo, Y., Guo, Y.L., Wang, L., Zhan, W.C., Wang, Y.S., et al., 2016. A highly-efficient La–MnO_x catalyst for propane combustion: the promotional role of La and the effect of the preparation method. *Catal. Sci. Technol.* 6, 8222–8233.
- Xu, Z.H., Yu, J.G., Jaroniec, M., 2015. Efficient catalytic removal of formaldehyde at room temperature using AlOOH nanoflakes with deposited Pt. *Appl. Catal. B* 163, 306–312.
- Yang, D.Y., Fu, S.Y., Huang, S.S., Deng, W., Wang, Y., Guo, L.M., et al., 2020. The preparation of hierarchical Pt/ZSM-5 catalysts and their performance for toluene catalytic combustion. *Microporous Mesoporous Mater.* 296, 109802.
- Yang, H.G., Deng, J.G., Liu, Y.X., Xie, S.H., Xu, P., Dai, H.X., 2016. Pt/Co₃O₄/3DOM Al₂O₃: highly effective catalysts for toluene combustion. *Chin. J. Catal.* 37, 934–946.
- Yin, H.F., Ma, Z., Chi, M.F., Dai, S., 2010. Activation of dodecanethiol-capped gold catalysts for CO oxidation by treatment with KMnO₄ or K₂MnO₄. *Catal. Lett.* 136, 209–221.
- Zhang, C.B., Liu, F.D., Zhai, Y.P., Ariga, H., Yi, N., Liu, Y.C., et al., 2012. Alkali-metal-promoted Pt/TiO₂ opens a more efficient pathway to formaldehyde oxidation at ambient temperatures. *Angew. Chem. Int. Ed.* 51, 9628–9632.
- Zhang, H.Y., Sui, S.H., Zheng, X.M., Cao, R.R., Zhang, P.Y., 2019. One-pot synthesis of atomically dispersed Pt on MnO₂ for efficient catalytic decomposition of toluene at low temperatures. *Appl. Catal. B* 257, 117878.
- Zhang, J.Y., Rao, C., Peng, H.G., Peng, C., Zhang, L., Xu, X.L., et al., 2018. Enhanced toluene combustion performance over Pt loaded hierarchical porous MOR zeolite. *Chem. Eng. J.* 334, 10–18.
- Zhang, S.S., Pu, W.H., Chen, A., Xu, Y.K., Wang, Y.Y., Yang, C.Z., et al., 2020. Oxygen vacancies enhanced photocatalytic activity towards VOCs oxidation over Pt deposited Bi₂WO₆ under visible light. *J. Hazard. Mater.* 384, 121478.
- Zhao, P.P., Chen, J., Yu, H.B., Cen, B.H., Wang, W.Y., Luo, M.F., et al., 2020a. Insights into propane combustion over MoO₃ promoted Pt/ZrO₂ catalysts: the generation of Pt–MoO₃ interface and its promotional role on catalytic activity. *J. Catal.* 391, 80–90.
- Zhao, S.Z., Wen, Y.F., Liu, X.J., Pen, X.Y., Lü, F., Gao, F.Y., et al., 2020b. Formation of active oxygen species on single-atom Pt catalyst and promoted catalytic oxidation of toluene. *Nano Res.* 13, 1544–1551.
- Zhou, S.H., Ma, Z., Yin, H.F., Wu, Z.L., Eichhorn, B., Overbury, S.H., et al., 2009. Low-temperature solution-phase synthesis of

- NiAu alloy nanoparticles via butyllithium reduction: influences of synthesis details and application as the precursor to active Au-NiO/SiO₂ catalysts through proper pretreatment. *J. Phys. Chem. C* 113, 5758–5765.
- Zhu, A.M., Zhou, Y., Wang, Y., Zhu, Q.L., Liu, H.Y., Zhang, Z.K., et al., 2018. Catalytic combustion of VOCs on Pt/CuMnCe and Pt/CeY honeycomb monolithic catalysts. *J. Rare Earths* 36, 1272–1277.
- Zou, S.B., Zhang, M.Y., Mo, S.P., Cheng, H.R., Fu, M.L., Chen, P.R., et al., 2020a. Catalytic performance of toluene combustion over Pt nanoparticles supported on pore-modified macro-meso-microporous zeolite foam. *Nanomaterials* 10, 30.
- Zou, X.L., Chen, J.F., Rui, Z.B., Ji, H.B., 2020b. Sequential growth reveals multi-spinel interface promotion for methane combustion over alumina supported palladium catalyst. *Appl. Catal. B* 273, 119071.